J Solid State Electrochem (2012) 16:35–44
DOI 10.1007/s10008-010-1271-x

ORIGINAL PAPER

PEO/P(VdF-HFP) blend based Li^+ ion-conducting composite polymer electrolytes dispersed with dedoped (insulating) polyaniline nanofibers

Ashok Kumar · Madhuryya Deka

Received: 23 July 2010 / Revised: 10 November 2010 / Accepted: 3 December 2010 / Published online: 22 December 2010

Abstract Composite polymer electrolyte membranes composed of poly(ethylene oxide) (PEO), poly(vinylidene fluoride-hexafluoropropylene) {P(VdF-HFP)} blends, dedoped (insulating) polyaniline (PAni) nanofibers, and $LiClO_4$ as salt have been synthesized with varying fraction of dedoped PAni nanofibers (from 2 to 10 wt.%). The ionic conductivity of PEO–P(VdF-HFP)–$LiClO_4$ electrolyte system increases with increase in the fraction of dedoped polyaniline nanofibers. This could be attributed to the incorporation of nanofibers (aspect ratio >50), which may provide high ion conducting path along the interface due to Lewis acid–base interactions between Li^+ ions and lone pair of electrons of nitrogen atom of polyaniline. However, at higher fraction (>6 wt.%), the nanofibers get phase separated from the polymer matrix and form domain-like structures, which may act as physical barrier to the conduction of Li^+ ions resulting in decreased ionic conductivity. Electrochemical potential window and interfacial stability of nanofibers dispersed polymer electrolyte membranes are also better than that of nanofibers free membranes.

Keywords Nanocomposites · Interface · Polymer electrolytes · XRD · Ionic conductivity

Introduction

The increasing energy needs of modern society have spurred all-embracing development and research in the field of polymer electrolytes for applications in various electrochemical devices particularly in solid-state rechargeable lithium batteries [1]. In batteries, being a separator membrane, polymer electrolyte must meet the requirements in terms of ionic conductivity, electrochemical performances, processibility, and safety. The most commonly studied polymer electrolyte membranes are complexes of Li salts with a high molecular weight polyethylene oxide (PEO) [2]. PEO excels as a polymer host because of its high solvating power for lithium ions and its compatibility with the lithium electrode [3]. However, high ionic conductivity (10^{-3}–10^{-4} S cm^{-1}) of most PEO-based polymer electrolytes is achieved at the temperature range of 80–100 °C [2–6], while at low temperature PEO is low conductive (10^{-7}–10^{-8} S cm^{-1}) because of the high crystallinity of PEO [5, 6].

Intensive efforts have been devoted to increase the ambient ionic conductivity of PEO-based polymer electrolytes [7]. A common approach is to add liquid plasticizers such as ethylene carbonate, propylene carbonate, diethyl carbonate etc. to the polymer matrix. These plasticized or gelled polymer electrolytes can exhibit ionic conductivity as high as 10^{-3} S cm^{-1} [8]. However, plasticized electrolytes exhibit drawbacks, such as increased reactivity with lithium metal electrode, solvent volatility, and poor mechanical properties at high degree of plasticization [7]. Another method to increase the ionic conductivity of PEO-based polymer electrolyte membranes is the addition of nano-scale inorganic fillers such as TiO_2, SiO_2, and Al_2O_3 [9–13]. The enhancement in ionic conductivity upon addition of nano-scale inorganic fillers has been interpreted assuming a specific role for ceramic fillers that not only prevents crystallization of polymer chains, but also promotes the interaction between the surface groups of the filler and the PEO segments [14, 15]. It has been reported

A. Kumar (✉) · M. Deka
Materials Research Laboratory, Department of Physics,
Tezpur University,
Napaam,
Tezpur, Assam 784028, India
e-mail: ask@tezu.ernet.in

that the interfacial stability of composite polymer electrolytes with lithium electrode is higher than that with filler-free polymer electrolytes [16].

Blending of different polymers provides easy preparation and control of the physical properties within the miscibility compositional regime and often exhibit properties that are superior to the properties of individual component of the blend [17–19]. Recently, many efforts have been devoted to increase the ionic conductivity of blend-based polymer electrolyte membranes such as P(VdF-HFP)/PVAc [20], PEO/PAN [21], and PVDF/PEO [22]. Fan et al. [23] reported that the blend of PEO and P(VdF-HFP) could hinder the crystallinity of PEO, and achieve a good combination of high ionic conductivity and good mechanical strength. Moreover, P(VdF-HFP) has excellent chemical stability due to VdF unit and plasticity due to HFP unit [24].

In the present work, we report a novel blend-based composite polymer electrolyte membrane by incorporating dedoped (insulating) polyaniline nanofiber into P(VdF-HFP)–PEO–$LiClO_4$ polymer electrolyte system. The fraction of dedoped polyaniline nanofibers has been varied keeping the PEO–P(VdF-HFP) ratio constant, and its effects on ionic transport and interfacial stability in P(VdF-HFP)–PEO–$LiClO_4$ polymer electrolyte have been investigated.

Experimental

Polyaniline nanofibers have been synthesized by the interfacial polymerization technique [25]. The interfacial polymerization reaction was carried out in 30-ml glass vials. One molar of aniline was dissolved in 10 ml of organic solvent (chloroform). Ammonium peroxydisulfate (0.25 M) was dissolved in 10 ml of double distilled water and 1 M dopant acid (H_2SO_4). The polyaniline nanofibers were dedoped with 1 M NaOH. The electronic conductivity of PAni nanofibers was measured with Keithley 2400 LV sourcemeter. We also employed four-probe method to measure the conductivity of doped and undoped nanofibers. This method contains four collinearly placed pointed stainless steel electrodes separated by a distance 1 cm, each which are made to contact the nanofiber samples. Current I is made to flow between the outer probes and voltage V is measured between the two inner probes. Since the contact area between the point probes and the sample is very small and a marginal distance separates the probes, local doping and dedoping of the sample can be omitted. The electronic conductivity of doped nanofibers was of the order of 10^{-4} S cm^{-1}, whereas after dedoping with base NaOH conductivity was found to be of the order of 10^{-11} S cm^{-1}. This confirms the insulating nature of dedoped PAni nanofibers.

The host polymer PEO (M_W=600,000), the co-polymer P(VdF-HFP) (M_W=400,000), and salt lithium perchlorate ($LiClO_4$) were received from Aldrich, USA. All the raw materials were heated at 50 °C under vacuum. Organic solvents acetonitrile and acetone were used as received from E-merck to prepare thin polymer electrolyte membranes by solution casting technique. Appropriate amount of PEO and salt $LiClO_4$ (O/Li=8) were dissolved in acetonitrile and then mixed together, stirred and heated at 50 °C. P(VdF-HFP), fixed at 40 wt.% of PEO for all samples, was stirred in presence of acetone at 50 °C. Subsequently, both the polymer solutions were mixed, stirred, and heated at 50 °C for 12–14 h. Dedoped polyaniline nanofibers were then added in the blend polymer solutions and allowed to stir for another 7–8 h. The viscous solution thus obtained was cast onto Petri dish and allowed to dry at room temperature. This procedure provided mechanically stable, free standing, and flexible membranes. The blend-based composite polymer electrolyte membranes used in this study were denoted as PEO–$LiClO_4$–P(VdF-HFP)–x% dedoped polyaniline nanofibers (x=0, 2, 4, 6, 8, 10).

The ionic conductivity of the membranes was determined from the complex impedance plots obtained by using a Hioki 3532-50 LCR HiTester in the frequency range 42 Hz to 5 MHz. A two-electrode system was employed for ionic conductivity measurements wherein the polymer electrolyte membrane was inserted between the two stainless steel electrodes. An ac sinusoidal signal of 3 mV with varying frequencies is applied across the cell and the impedance modulus and phase shift of the electrode/electrolyte/electrode cell assembly were measured. The nature of conductivity of nanofibers dispersed polymer electrolytes was determined by Wagner polarization technique with polymer electrolyte between graphite blocking electrodes. The transference number was found to be 0.97 indicating that conductivity was essentially ionic in nature. X-ray diffractograms were studied by Rigaku miniflex X-ray diffractometer. Surface morphology of the composite electrolytes was studied by using scanning electron microscope (Jeol model JSM 6390 LV). Fourier transform infrared spectroscopy (FTIR) studies were carried out using Nicolet Impact 410 spectrophotometer. The diameter of polyaniline nanofibers was measured by TEM (JEOL-TEM-100 CXII). The average diameter and length of the fibers are found to be 20–30 and 1,000 nm as reported in our previous work [26]. Linear sweep voltammetry curve was obtained using electrochemical workstation (Sycopel AEW 2, UK). The electrochemical cell in this case was comprised of stainless steel working electrode and lithium metal as a reference electrode and the voltage was swept between the potential ranges from 2 to 6 V with a scan rate 0.1 mVs^{-1}. The interfacial stability of nanocomposite

polymer electrolytes was studied by fabricating Li/polymer electrolyte/Li cells at room temperature and was monitored for 15 days.

Results and discussion

TEM studies

Figure 1 shows the TEM micrograph of PAni nanofibers. From the figure it is observed that nanofiber is composed of randomly packed polymer chains. As the PAni nanofibers are synthesized by interfacial polymerization, no over-growth of polyaniline on the nanofiber scaffolds does take place and nanofibrillar morphological units are formed. The diameter and length of the fibers are found to be 20 to 30 nm and more than 1,000 nm, respectively.

X-ray diffraction studies

X-ray diffraction patterns of pure PEO, P(VdF-HFP), and dedoped polyaniline nanofibers are presented in Fig. 2. High intensity peaks at 2θ=20° and 2θ=23° are observed in the XRD pattern of dedoped polyaniline nanofibers (Fig. 2c). The peaks at 2θ=20° and 38° correspond to (020) and (202) crystalline peaks of P(VdF-HFP). This confirms the partial crystallization of PVdF units in the copolymer and semi-crystalline structure of P(VdF-HFP) [27]. PEO shows a characteristic peak at 2θ=19° (Fig. 2a). Figure 3 shows the XRD patterns of PEO–P(VdF-HFP)–$LiClO_4$–x% dedoped polyaniline nanofibers composite polymer electrolytes. It is observed that when P(VdF-HFP) is blended with PEO, no additional peak appears; only the intensity of crystalline peaks slightly decreases and broadens as compared to pure PEO suggesting that the amorphicity

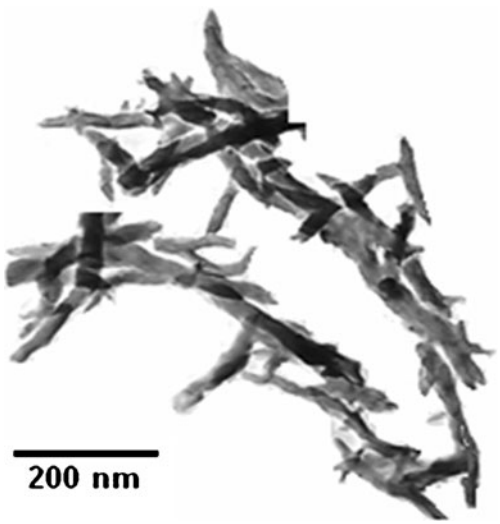

Fig. 1 TEM image of dedoped polyaniline nanofibers

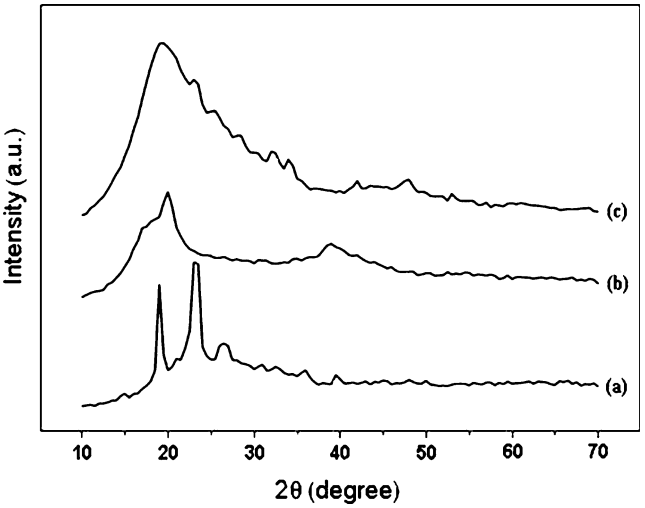

Fig. 2 XRD patterns of (*a*) PEO, (*b*) P(VdF-HFP), (*c*) dedoped polyaniline nanofibers

increases [28]. When dedoped polyaniline nanofibers are incorporated in the PEO–P(VdF-HFP)–$LiClO_4$ the crystalline peak further broadens while the intensity of the small peak at 2θ=39° decreases significantly as shown in Fig. 3b–f. The degree of crystallinity is determined by a method described elsewhere [29]. Calculated values of degree of crystallinity with increasing fraction of dedoped PAni nanofibers are given in Table 1. It is observed that the degree of crystallinity decreases with increasing nanofibers content and reaches a minimum at 6 wt.% nanofibers fraction. This reduction in crystallinity upon addition of nanofibers is attributed to the suppression of the reorganization of polymer chains by the nanofibers [30]. However, at higher fraction of nanofibers (>6 wt.%), the degree of

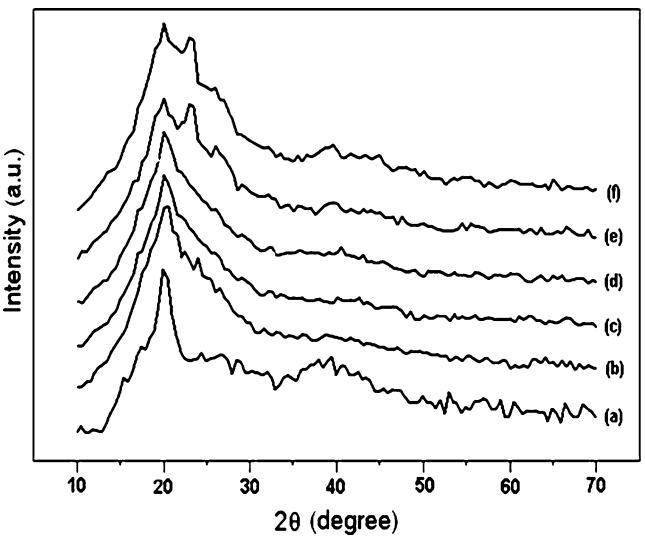

Fig. 3 XRD patterns of PEO–P(VdF-HFP)–$LiClO_4$–x% dedoped polyaniline nanofibers polymer electrolyte membranes (*a*) x=0, (*b*) x=2, (*c*) x=4, (*d*) x=6, (*e*) x=8, and (*f*) x=10

Table 1 Degree of crystallinity of PEO–P(VdF-HFP)–$LiClO_4$–x % dedoped polyaniline nanofibers polymer electrolytes at different concentration of polyaniline nanofibers

Concentration of dedoped PAni nanofibers (wt.%)	Degree of crystallinity (%)
0	34.5
2	30.1
4	25.4
6	19.3
8	21.7
10	27.3

crystallinity increases with increasing nanofibers content indicating that crystalline phase starts increasing above 6 wt.% of nanofibers fraction due to reorganization of polymer chains in PEO–P(VdF-HFP)–$LiClO_4$ electrolyte system. At 8 and 10 wt.% of nanofibers fraction an additional peak appears at $2\theta=23°$, which can be assigned to dedoped polyaniline nanofibers suggesting that above 15 wt.% polyaniline nanofibers get phase separated from the PEO–P(VdF-HFP)–$LiClO_4$ polymer electrolyte phase.

Ionic conductivity measurements

The complex impedance plots for PEO–P(VdF-HFP)–$LiClO_4$ polymer electrolyte membranes with different weight fraction of polyaniline nanofibers are presented in Fig. 4a–f. All plots comprise a semicircular arc in the high-frequency region and an oblique line in the low-frequency region. The ionic conductivity is calculated from the relation $\sigma=l/R_b r^2\pi$; where l and r are thickness and radius of the sample membrane disks and R_b is the bulk resistance. The value of the bulk resistance (R_b) was extracted from the point where the high-frequency semicircles intercept the abscissa (Z'). The thickness of the nanocomposite films was found to be in the range from 350 to 400 μm while the area was 0.785 cm^2, which is the area of the sample membrane disk. This response of the electrode/electrolyte/electrode cell assembly can be simulated as an equivalent circuit comprising a combination of a bulk resistance "R_b" of the sample in parallel with its geometrical capacitance "C_g" in series with a constant phase element (CPE) consisting of a double-layer interfacial capacitor C_{dl} and a charge transfer resistance [31]. The total impedance of the equivalent circuit at frequency ω can be written as:

$$Z_{\text{Total}} = \left[\frac{1}{1+\left(\omega R_b C_g\right)^2}\right] - jR_b\left[\frac{\omega R_b C_g}{1+\left(\omega R_b C_g\right)^2}\right] + \frac{1}{\omega C_{dl}} \quad (1)$$

At high frequencies when the reactance and the bulk resistance of the sample are comparable, i.e., $\frac{1}{\omega C_g} \approx R_b$, parallel combination of bulk resistance R_b and capacitance C_g contribute dominantly to the overall impedance which gives rise to a semicircle [31]. At low frequencies when $\frac{1}{\omega C_g} \leq R_b$, the contribution of C_g becomes negligible to the overall impedance and the equivalent circuit behaves as a series combination of R_b and constant phase element giving an inclined spike displaced by R_b on the abscissa of the impedance plot. However, a 90° line in addition to the semicircle is obtained for perfectly smooth surfaces. The slope of the line decreases with increasing roughness. The CPE mentioned above has been modeled to account for the semicircle flattening and spike tilting as observed in the Nyquist plot. It may be considered as a leaky capacitor where current is not exactly ahead of voltage by 90° as in ideal capacitor. The physical origin of CPE for polymer electrolytes is related to the presence of crystalline nonconducting regions interconnected with conducting amorphous material within the PEO spherulites [32]. Inset of Fig. 4 shows the equivalent circuit for the impedance spectra obtained in this study. The impedance of CPE is given by

$$Z_{\text{CPE}} = k(j\omega)^{-p} \text{where } 0 < p < 1 \quad (2)$$

When $p=0$, Z is frequency independent, and k is just the resistance and when $p=1$, $Z=k/j\omega=-j/\omega(k)$, the constant k^{-1} now corresponds to the capacitance. When p is between 0 and 1, the CPE acts in a way intermediate between a resistor and a capacitor. The series CPE terms tilt the spike

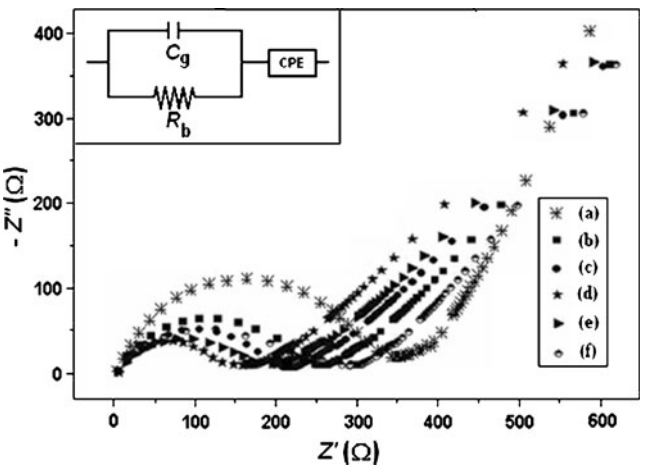

Fig. 4 Complex impedance spectra of PEO–P(VdF-HFP)–$LiClO_4$–x % dedoped polyaniline nanofibers polymer electrolyte membranes (*a*) $x=0$, (*b*) $x=2$, (*c*) $x=4$, (*d*) $x=6$, (*e*) $x=8$, and (*f*) $x=10$. *Inset* shows the equivalent circuit representing the actual cell assembly

and parallel CPE terms broaden the semicircle [32]. The values for R_b and C_g estimated from Nyquist plots are presented in Table 2. The bulk resistance (R_b) for nanofiber free polymer electrolyte is estimated to be ~341 Ω at room temperature, which decreases significantly upon addition of PAni nanofiber in the PEO/P(VdF-HFP)/$LiClO_4$ complex. On the other hand, the values for geometrical capacitance (C_g) for all compositions are in the range of nF, which implies that the high-frequency semicircles arise due to bulk of the material. Variation of ionic conductivity with increasing fraction of nanofibers is shown in Fig. 5. It is observed that the σ_{ionic} increases with the increase of weight fraction of nanofibers. Maximum conductivity was found to be 3.1×10^{-4} S cm^{-1} at room temperature for 6 wt. % dedoped polyaniline nanofiber fillers, which is over seven times higher as compared to that (4.5×10^{-5} S cm^{-1}) for polymer electrolyte without nanofibers. However, as the filler (dedoped nanofibers) fraction increases beyond 6 wt. %, the ionic conductivity decreases.

The enhancement of up to 6 wt.% of nanofibers content seems to be correlated with the fact that the dispersion of dedoped polyaniline nanofibers to PEO–P(VdF-HFP) prevents polymer chain reorganization due to the high aspect ratio (>50) of nanofibers, resulting in reduction in polymer crystallinity, which gives rise to an increase in ionic conductivity. The increase in ionic conductivity may also result from Lewis acid–base interaction [33–36]. In the present composite polymer electrolytes, the oxygen atom in PEO has two lone pair of electrons and nitrogen atom in PAni nanofibers has one lone pair of electrons, which act as strong Lewis base centers and Li^+ cations as strong Lewis acid giving rise to numerous acid–base complexes in the composite polymer electrolyte. Accordingly, three types of Lewis acid–base complexes can be formed [37]. First type of complexes involve PEO–Li^+–PEO interaction, which leads to the transient cross-linking of PEO chains via Li^+ cations resulting in the reduction of ionic conductivity. Second type of interaction is due to mixed PEO–Li^+–PAni nanofibers complexes, which involves Lewis base oxygen from PEO chain and Lewis base nitrogen from polyaniline. The third type of interaction involves only the Lewis base nitrogen from polyaniline and Li^+ cations. The formation of second and third type of complexes leads to lowering of concentration of first type of complexes and hence density of transient cross-linking is reduced. [37]. This allows mobile ions to move more freely either on the surface of the nanofibers or through a low-density polymer phase at the interface, which results in enhanced ionic conductivity. The reduction in crystallinity upon addition of polyaniline nanofibers up to 6 wt.% is consistent with XRD results. Enhancement in ionic conductivity can also be attributed to the creation of polymer–filler interface. The filler–polymer interface is a site of high defect concentration providing channels for faster ionic transport [38] and the structure and chemistry of filler–polymer interface may have even more important role than the formation of amorphous phase in the electrolyte.

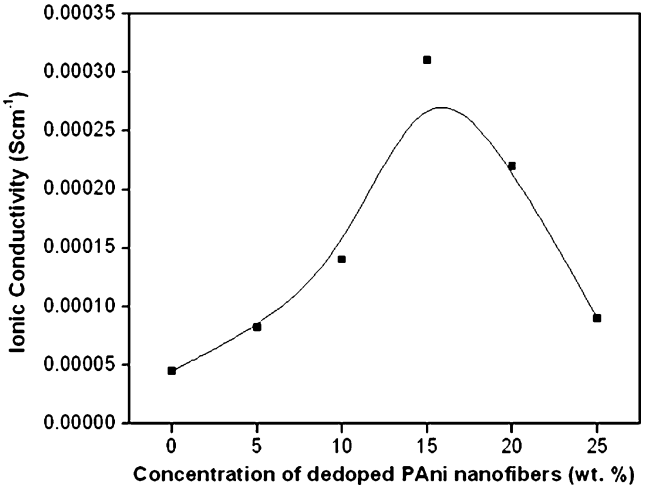

Fig. 5 Variation of ionic conductivity with different weight fraction of dedoped polyaniline nanofibers

On the other hand, the decrease in ionic conductivity for fraction of nanofibers higher than 6 wt.% can be attributed to the blocking effect on the transport of charge carriers resulting from the phase separation of nanofibers [39]. Besides, above 6 wt.% a depressed semicircle is seen in the impedance spectra, which is characteristic of a system where more than one conduction processes are present simultaneously [40]. SEM micrographs show that, at higher weight fraction of nanofibers (6 wt.%), a two-phase microstructure is observed. This could be attributed to the fact that at higher fraction of nanofibers, uniform dispersion of nanofibers in PEO–P(VdF-HFP) matrix is difficult to

Table 2 Values of bulk resistance (R_b) and geometrical capacitance (C_g) for different weight fraction of dedoped PAni nanofibers in PEO/P(VdF-HFP)/$LiClO_4$ complex estimated from observed impedance spectra

wt.% of dedoped PAni nanofibers	Bulk resistance, R_b (Ω)	Capacitance, C_g (nF)
0	341	4.5
2	234	2.9
4	215	3.7
6	143	2.1
8	182	3.2
10	254	4

achieve due to formation of phase-separated morphologies. This is expected to affect the conductivity of the system, since a large number of Li^+ cations are trapped in the phase separated nanofibers. Thus, the decrease of ionic conductivity above 6 wt.% nanofibers content can be attributed to the effect of phase separation, which is consistent with the XRD and SEM results.

Figure 6 shows the conductivity versus temperature inverse plots of polymer electrolyte films in the temperature range from 25 to 80 °C. The figure shows that the ionic conduction in nanocomposite polymer electrolytes obeys the Arrhenius relation with two degree of slopes:

$$\sigma = \sigma_0 exp(-E_a/kT) \quad (3)$$

where σ, σ_0, E_a, k, and T are the ionic conductivity, the pre-exponential factor, the activation energy, the Boltzmann constant, and the absolute temperature, respectively [41, 42]. All the samples show a break point at around 60 °C, near the melting temperature of PEO, reflecting the well-known transition from PEO crystalline to amorphous phase. As expected the increase in temperature leads to increase in ionic conductivity because as the temperature increases the polymer chains flex at increased rate to produce larger free volume, which leads to enhanced polymer segmental and ionic mobilities. The enhancement of ionic conductivity by the dedoped polyaniline nanofibers can be explained by the fact that the nanofibers inhibit the recrystallization kinetics, helping to retain the amorphous phase down to relatively low temperatures [43].

Scanning electron microscopy studies

The SEM micrographs for PEO–P(VdF-HFP)–$LiClO_4$–x% dedoped polyaniline nanofibers membranes are presented in Fig. 7a–f. In general, three-four phases are known to coexist in the PEO-based polymer electrolytes viz. crystalline PEO phase, crystalline PEO–Li salt complex phase, and amorphous PEO phase. It is observed that below 6 wt.% nanofibers content in PEO–P(VdF-HFP) matrix (Fig. 7a–c), the surface morphology is granular and smooth, which could be attributed to the reduction of PEO crystallinity due to complexation with lithium salt and polyaniline nanofibers. At 6 wt.%, rough morphology and sharp interfaces are observed (Fig. 7d) which may facilitate lithium ion conduction along the interface [44].

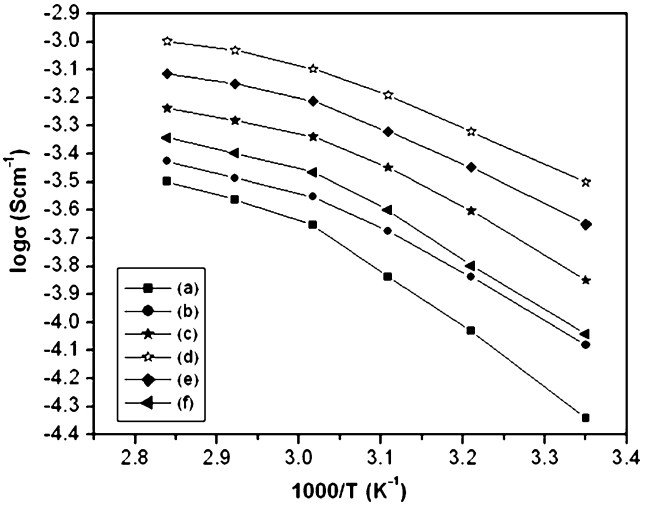

Fig. 6 logσ vs. temperature inverse curve PEO–P(VdF-HFP)–$LiClO_4$–x% dedoped polyaniline nanofibers polymer electrolyte membranes (*a*) x=0, (*b*) x=2, (*c*) x=4, (*d*) x=6, (*e*) x=8, and (*f*) x=10

Figure 7e shows a two-phase microstructure, marked by circles, at 8 wt% of nanofibers content due to phase segregation of nanofibers. Phase separation becomes more prominent at 10 wt.% of nanofibers as shown in Fig. 7f. The nanofibers get phase separated from the PEO–P(VdF-HFP) polymer matrix and form domain-like regions, which may act as physical barriers to the effective motion of the ions leading to decrease in ionic conductivity.

FTIR analysis

FTIR is a powerful tool to characterize the chain structure of polymers and has led the way in interpreting the reactions of multifunctional monomers including rearrangements and isomerizations [45, 46]. FTIR spectra of $LiClO_4$, dedoped polyaniline nanofibers, P(VdF-HFP), PEO, and polymer complexes are shown in Fig. 8. The symmetric and asymmetric C–H stretching vibrations of pure P(VdF-HFP) are observed at 3,000 cm^{-1}. Frequencies 1,286–1,066 cm^{-1} are assigned to –C–F– and –CF_2– stretching vibration of P(VdF-HFP). Frequency 883 cm^{-1} is assigned to vinylidene group of polymer. Stretching and bending modes of $(CH_2)_\alpha$ for pure PEO are observed at 1,470.25 and 1,353.91 cm^{-1}, respectively. The peak at 1,104.2 cm^{-1} is assigned to ν (C–O–C) of PEO molecule [47]. Frequency 1,120 cm^{-1} is assigned to the in-plane C–H bending of polyaniline nanofibers [48]. The ammonium ion displays broad absorption in the frequency region 3,350–3,050 cm^{-1} because of N–H stretching vibration. The N–H bending vibration of secondary aromatic amine of polyaniline nanofibers occurs at 1,507 cm^{-1}. The frequency 1,650 cm^{-1} of polyaniline nanofibers is assigned to C=C of aromatic ring.

The assigned peaks of dedoped polyaniline nanofibers get shifted towards lower frequency after incorporation into the polymer electrolyte system signifying their effect on the electrolyte system. The peak for in-plane C–H bending of polyaniline nanofibers at 1,120 cm^{-1} is shifted to 1,170 cm^{-1} for 2 wt.% and to 1,185 cm^{-1} for 6 wt.% of dedoped nanofibers. The peak at 1,507 cm^{-1} due to N–H bending vibration of secondary aromatic amine of polyaniline nanofibers gets shifted in case of

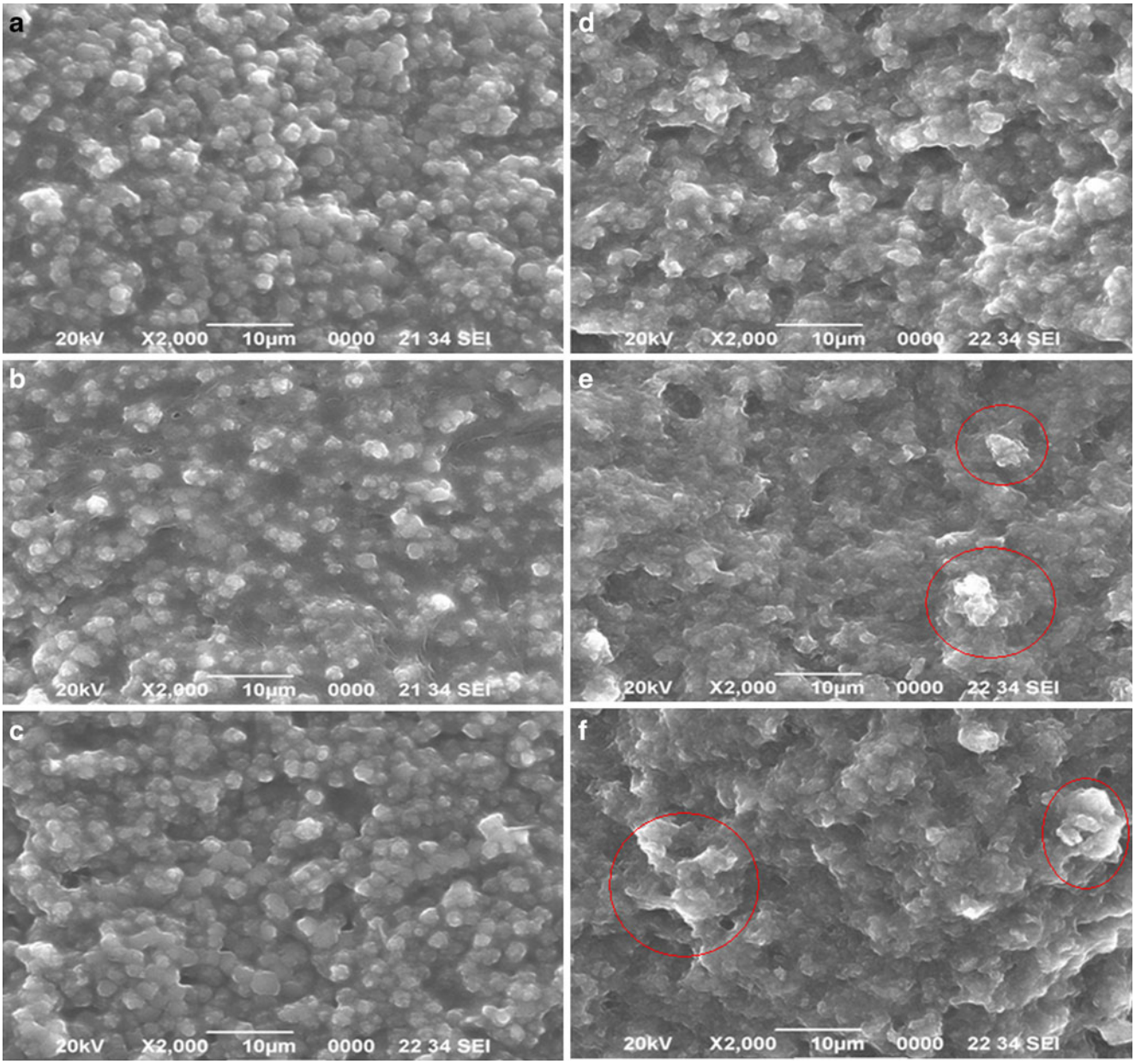

Fig. 7 SEM micrographs of PEO–P(VdF-HFP)–$LiClO_4$–*x*% dedoped polyaniline nanofibers polymer electrolytes **a** $x=0$, **b** $x=2$, **c** $x=4$, **d** $x=6$, **e** $x=8$, and **f** $x=10$

composite polymer electrolytes to 1,550 cm^{-1} (for 2 wt.%) and 1,580 cm^{-1} (for 6 wt.%). The peaks at 1,690 cm^{-1} (for 2 wt.%) and 1,730 cm^{-1} (for 6 wt.%) are evidence of shifting of C=C of aromatic ring peak (1,650 cm^{-1}) of pure dedoped polyaniline nanofibers. However, FTIR spectra of PEO–P(VdF-HFP) polymer electrolyte containing 8 wt.% of dedoped nanofibers show all the peaks of the dedoped nanofibers at their original assigned positions. This result strongly corroborates the occurrence of phase separation at higher fraction of nanofibers (>6 wt.%) and is consistent with XRD and SEM results.

Electrochemical studies

Figure 9 displays the current–voltage response obtained for PEO–$LiClO_4$, PEO–P(VdF-HFP)–$LiClO_4$, and PEO–P(VdF-HFP)–$LiClO_4$–6 wt.% dedoped polyaniline nanofibers composite. The onset of current identifies the anodic decomposition voltage of the electrolytes. It is observed that PEO–$LiClO_4$ shows decomposition voltage at 4.3 V whereas after blending with P(VdF-HFP), the decomposition voltage is slightly increased (4.4 V). However, after incorporation of dedoped PAni nanofibers (6 wt.% in this case) in the blend system, the value of decomposition

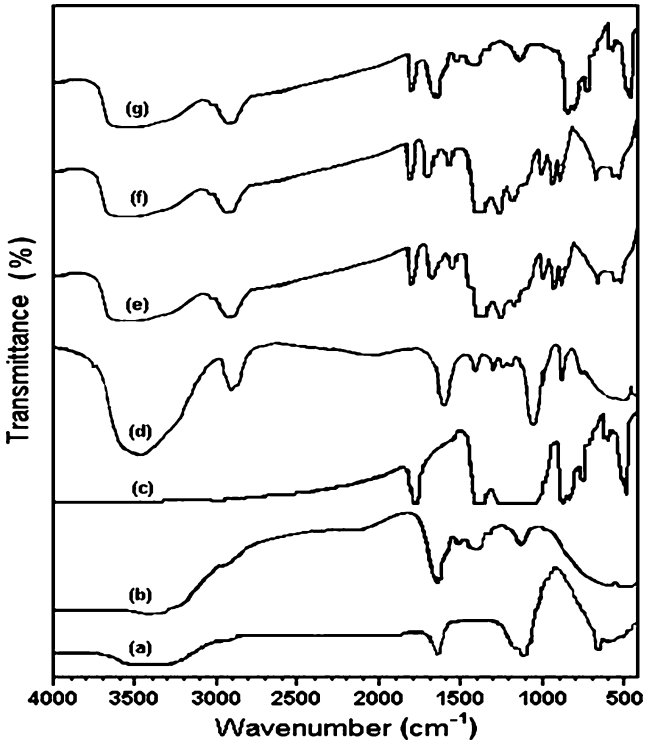

Fig. 8 FTIR spectra of (*a*) $LiClO_4$, (*b*) dedoped polyaniline nanofibers, (*c*) P(VdF-HFP), (*d*) PEO, (*e*) PEO–P(VdF-HFP)–$LiClO_4$–2 wt.% dedoped polyaniline nanofibers, (*f*) PEO–P(VdF-HFP)–$LiClO_4$–6 wt.% dedoped polyaniline nanofibers, and (*g*) PEO–P(VdF-HFP)–$LiClO_4$–8 wt.% dedoped polyaniline nanofibers

voltage increases significantly and sets at about 4.8 V. Thus, there is a clear improvement in the voltage stability factor in the electrolyte films containing dedoped PAni nanofibers. This value of working voltage range (i.e., electrochemical potential window) appears to be high enough to use the nanocomposite polymer electrolyte films as a solid-state separator/electrolyte in Li batteries.

Compatibility of nanocomposite polymer electrolyte with electrode materials is an important factor for polymer battery applications. Due to the reactivity of electrode materials, most of the polymer electrolytes passivate lithium, which result in the formation of a non-uniform solid electrolyte interface (SEI) layer [26]. Formation of this passivation layer increases the resistance to the flow of ions through the interface resulting in the decrease in overall current in the circuit, i.e., through the electrolyte. The decrease in conductivity is essentially a decrease in the conductance of the electrolyte due to formation of SEI layer. The interfacial stability is a measure of resistance to the formation of SEI layer. In order to examine the interfacial stability of polymer electrolytes before and after incorporating dedoped polyaniline nanofibers, the ionic conductivity was measured by fabricating Li/polymer electrolyte membrane/Li cells at room temperature and monitored for 15 days. Three systems viz. PEO–$LiClO_4$, PEO–P(VdF-HFP)–$LiClO_4$, and PEO–P(VdF-HFP)–$LiClO_4$–6 wt.% dedoped PAni nanofibers have been selected for the compatibility study and the results are shown in Fig. 10. It reveals that ionic conductivity of all the electrolyte systems decreases with time but decrease of ionic conductivity in PEO–$LiClO_4$ electrolyte is much larger than the other two systems. It is well known that PEO–$LiClO_4$ exhibits highly crystalline structure at room temperature. The existence of crystallites in PEO–$LiClO_4$ affects the charge transfer reaction because the interface between the lithium electrode and crystalline polymer

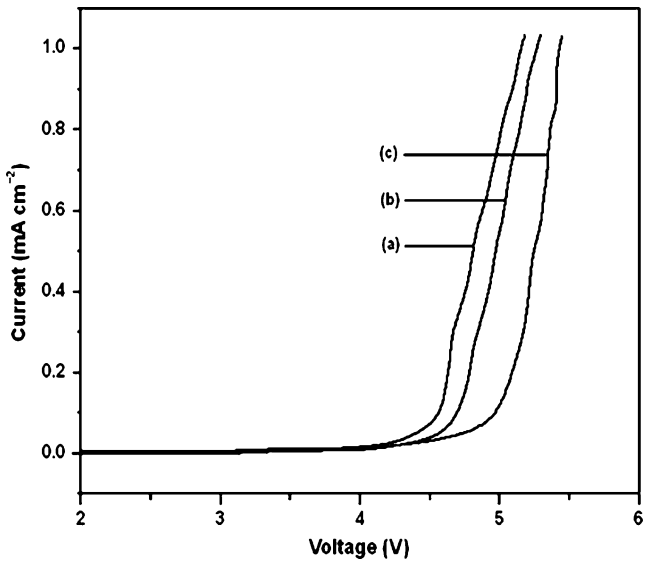

Fig. 9 Linear sweep voltammetry plots of (*a*) PEO–$LiClO_4$, (*b*) PEO–P(VdF-HFP)–$LiClO_4$, and (*c*) PEO–P(VdF-HFP)–$LiClO_4$–6 wt.% dedoped polyaniline nanofibers

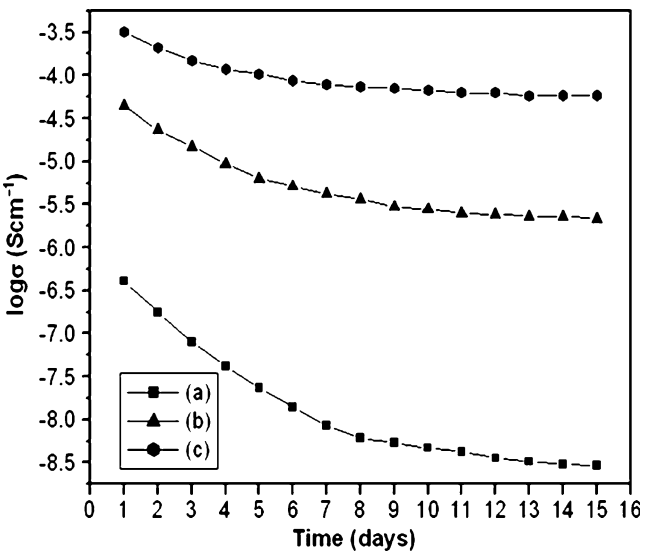

Fig. 10 Interfacial stability of (*a*) PEO–$LiClO_4$, (*b*) PEO–P(VdF-HFP)–$LiClO_4$, and (*c*) PEO–P(VdF-HFP)–$LiClO_4$–6 wt.% dedoped polyaniline nanofibers

function as a barrier for electrochemical reaction of lithium [49], which gives rise to increase in interfacial resistance. When PEO is blended with P(VdF-HFP) the crystallinity of the system is greatly reduced, as confirmed by XRD results, resulting in higher interfacial stability than PEO–$LiClO_4$. On the other hand, PEO–P(VdF-HFP)–$LiClO_4$–6 wt.% dedoped PAni nanofibers membrane shows highest interfacial stability (Fig. 8c). The highest interfacial stability of nanofibers dispersed polymer electrolyte seems to be associated with the fact that the high aspect ratio (>50) nanofibers form a barrier layer at the electrode, which effectively impedes the electrode–electrolyte reaction [28, 50]. This in turn reduces the passivation layer on the electrode leading to better interfacial stability between electrode and electrolyte.

Conclusions

Polymer electrolytes nanocomposite membranes based on PEO–P(VdF-HFP)–$LiClO_4$ with dedoped polyaniline nanofibers have been developed and investigated. The ac impedance analysis shows that the ionic conductivity of the polymer electrolyte membranes increases when dedoped polyaniline nanofibers are added as filler up to a fraction of 6 wt.%. XRD results show a gradual decrease in degree of crystallinity with increase in dedoped polyaniline nanofibers up to 6 wt.%. At higher fraction (>6 wt.%) the polyaniline nanofibers get phase separated from the polymer matrix as revealed by the occurrence of new peaks in the XRD spectra. SEM studies reveal two-phase morphology above 6 wt.% nanofibers indicating the phase separation of polyaniline nanofibers. FTIR spectra also confirm the phase separation at nanofibers fraction greater than 6 wt.% showing peaks for dedoped polyaniline nanofibers at their assigned positions. The three moieties PEO, P(VdF-HFP), and dedoped polyaniline nanofibers no longer remain a miscible uniform phase and nanofibers get phase separated from the polymer matrix giving the domain-like structures. These domains may create barrier in the conduction path leading to the decrease in ionic conductivity. The interfacial stability of the nanofibers dispersed composite polymer electrolytes is observed to be better than that of PEO–P(VdF-HFP)–$LiClO_4$ and PEO–$LiClO_4$. Incorporation of dedoped (insulating) nanofibers up to a critical fraction increases the ionic conductivity of the polymer electrolyte system making them new promising potential membrane for lithium rechargeable batteries.

Acknowledgment The authors would like to thank Mr. A.K. Nath and Mr. Somik Banerjee, Department of Physics, Tezpur University, for their help in synthesis and making measurements during the course of this work.

References

1. Tarascon JM, Armand M (2001) Issues and challenges facing rechargeable lithium batteries. Nature (London) 414:359–367
2. Ahn J-H, Wang GX, Liu HK, Dou SX (2003) Nanoparticle-dispersed PEO polymer electrolytes for Li batteries. J Power Sources 119–121:422–426
3. Algamir M, Abraham KM (1994) Lithium batteries, new materials, development and prospectives. In: Pistoia G (ed) Industrial chemistry library, vol 5. Elsevier, Amsterdam, pp 93–136
4. Abraham KM (1993) Highly conductive polymer electrolytes. In: Scrosati B (ed) Applications of electroactive polymers. Chapman and Hall, London, pp 75–112
5. Kovac M, Gaberscek M, Grdadolnik J (1998) The effect of plasticizer on the microstructural and electrochemical properties of a $(PEO)_nLiAl(SO_3\ Cl)_4$ system. Electrochim Acta 44:863–870
6. Armand MB, Chabagno JM, Duclot MJ (1997) Fast ion transport in solids. In: Vashista P, Shenoy GK (eds) Elsevier. North-Holland, New York, pp 131–136
7. Jacob MME, Hackett E, Giannelis EP (2003) From nanocomposite to nanogel polymer electrolytes. J Mater Chem 13:1–5
8. Song JY, Wang YY, Wan CC (1999) Review of gel-type polymer electrolytes for lithium-ion batteries. J Power Sources 77:183–197
9. Fan LZ, Nan C-W, Zhau SJ (2003) Effect of modified SiO_2 on the properties of PEO-based polymer electrolytes. Solid State Ion 164:81–86
10. Zhang S, Lee JY, Hong L (2004) Visualization of particle distribution in composite polymer electrolyte systems. J Power Sources 126:125–133
11. Nookala M, Kumar B, Rodrigues S (2002) Ionic conductivity and ambient temperature Li electrode reaction in composite polymer electrolytes containing nano-size alumina. J Power Sources 111:165–172
12. Qian XM, Gu NY, Cheng ZL, Yang XR, Wang EK, Dong SJ (2001) Impedance study of $(PEO)_{10}LiClO_4$–Al_2O_3 composite polymer electrolyte with blocking electrodes. Electrochim Acta 46:1829–1836
13. Liu Y, Lee JY, Hong L (2003) Morphology, crystallinity, and electrochemical properties of in situ formed poly(ethylene oxide)/TiO_2 nanocomposite polymer electrolytes. J Appl Polym Sci 89:2815–2822
14. Croce F, Persi L, Scrosati B (2000) Impedance spectroscopy study of PEO-based nanocomposite polymer electrolytes. J Electrochem Soc 147:1718–1721
15. Croce F, Appetecchi GB, Curini R, Martinelli A, Persi L, Ronci F, Scrosati B, Caminiti R (1999) Physical and chemical properties of nanocomposite polymer electrolytes. J Phys Chem B 103:10632–10638
16. Croce F, Appetecchi GB, Persi L, Scrosati B (1998) Nanocomposite polymer electrolytes for lithium batteries. Nature 394:456–458
17. Tang M, Liau WR (2000) Solvent effect on the miscibility of poly (4-hydroxystyrene)–poly(ethylene oxide) blends. Eur Polym J 36:2597–2603
18. Pielichowski K, Hamerton I (2000) Compatible poly(vinyl chloride)/chlorinated polyurethane blends: thermal characteristics. Eur Polym J 36:171–181
19. Rocco AM, Pereira RP, Felisberti MI (2001) Miscibility, crystallinity and morphological behavior of binary blends of poly (ethylene oxide) and poly(methyl vinyl ether–maleic acid). Polymer 42:5199–5205
20. Choi N-S, Lee Y-G, Park J-K, Ko J-M (2001) Preparation and electrochemcial characteristics of plasticized polymer electrolytes

based upon a P(VdF-co-HFP)/PVAc blend. Electrochim Acta 46:1581–1586
21. Choi BK, Kim YW, Shin HK (2000) Ionic conduction in PEO–PAN blend polymer electrolytes. Electrochim Acta 45:1371–1374
22. Jacob MME, Prabaharan SRS, Radhakrishna S (1997) Effect of PEO addition on the electrolytic and thermal properties of PVDF-$LiClO_4$ polymer electrolytes. Solid State Ion 104:267–276
23. Fan L, Dang Z, Nan C-W, Li M (2002) Thermal electrical and mechanical properties of plasticized polymer electrolytes based on PEO/P(VDF-HFP) blends. Electrochim Acta 48:205–209
24. Arvindan V, Vickraman P (2007) Polyvinylidenefluoride-hexafluoropropylene based nanocomposite polymer electrolytes (NCPE) complexed with $LiPF_3$ (CF_3 CF_2)$_3$. Eur Polym J 43:5121–5127
25. Huang J (2006) Syntheses and applications of conducting polymer polyaniline nanofibers. Pure Appl Chem 78:15–27
26. Deka M, Nath AK, Kumar A (2009) Effect of dedoped (insulating) polyaniline nanofibers on the ionic transport and interfacial stability of poly(vinylidenefluoride-hexafluoropropylene) based composite polymer electrolyte membranes. J Membr Sci 327:188–194
27. Saikia D, Kumar A (2004) Ionic conduction in P(VDF-HFP)/PVDF-(PC+DEC)-$LiClO_4$ polymer gel electrolytes. Electrochim Acta 49:2581–2589
28. Leo CJ, Rao GVS, Chowdari BVR (2002) Studies on plasticized PEO–lithium triflate-ceramic filler composite electrolyte system. Solid State Ion 148:159–171
29. Saikia D, Hussain AMP, Kumar A, Singh F, Avasthi DK (2006) Ionic conduction studies in Li^{3+} ion irradiated (PVDF-HFP)-(PC+DEC)-$LiCF_3SO_3$ gel polymer electrolytes. NIMB 244:230–234
30. Scrosati B, Croce F, Panero S (2001) Progress in lithium polymer battery R&D. J Power Sources 100:93–100
31. Stephan AM, Thirunakaran R, Renganathan NG, Sundaram V, Pitchumani S, Muniyandi N, Gangadharan R, Ramamoorthy P (1997) A study on polymer blend electrolyte based on PVC/PMMA with lithium salt. J Power Sources 81–82:752–758
32. Deka M, Kumar A (2010) Enhanced electrical and electrochemical properties of PMMA–clay nanocomposite gel polymer electrolytes. Electrochim Acta 55:1836–1842
33. Rajendran S, Uma T (2000) Conductivity studies on PVC/PMMA polymer blend electrolyte. Mater Lett 44:242–247
34. Croce F, Persi L, Scrosati B, Serraino-Fiory F, Plichta E, Hendrickson MA (2001) Role of the ceramic fillers in enhancing the transport properties of composite polymer electrolytes. Electrochim Acta 46:2457–2461
35. Chung SH, Wang Y, Persi L, Croce F, Greenbaum SG, Scrosati B, Plichta E (2001) Enhancement of ion transport in polymer electrolytes by addition of nano-scale inorganic oxides. J Power Sources 97–98:644–648
36. Stephan AM, Nahm KS (2006) Review on composite polymer electrolytes for lithium batteries. Polymer 47:5952–5964
37. Wieczorek W, Zalewska A, Raducha D, Florjańczyk Z, Stevens JR (1996) Polyether, poly(*N*, *N*-dimethylacrylamide), and LiClO4 composite polymeric electrolytes. Macromolecules 29:143–155
38. Kumar B, Scanlon LG (1994) Polymer-ceramic composite electrolytes. J Power Sources 52:261–268
39. Kim S, Park S-J (2007) Preparation and electrochemical behaviors of polymeric composite electrolytes containing mesoporous silicate fillers. Electrochim Acta 52:3477–3484
40. Kurian M, Galvin ME, Trapa PE, Sadoway DR, Mayes AM (2005) Single-ion conducting polymer–silicate nanocomposite electrolytes for lithium battery applications. Electrochim Acta 50:2125–2134
41. Li ZH, Su GY, Wang XY, Gao DS (2005) Micro-porous P(VDF-HFP)-based polymer electrolyte filled with Al_2O_3 nanoparticles. Solid State Ion 176:1903–1908
42. Christie AM, Lilly SJ, Staunton E, Andreev YG, Bruce PG (2005) Increasing the conductivity of crystalline polymer electrolytes. Nature 433:500–553
43. Rhoo H-J, Kim H-T, Park J-K, Hwang T-S (1997) Ionic conduction in plasticized PVC/PMMA blend polymer electrolytes. Electrochim Acta 42:1571–1579
44. Saikia D, Kumar A (2005) Ionic transport in P(VDF-HFP)-PMMA-$LiCF_3SO_3$-(PC+DEC)-SiO_2 composite gel polymer electrolyte. Eur Polym J 41:563–568
45. Pavia DL, Lampman GM, Kriz GS (2001) Introduction to spectroscopy, 3rd edn. Harcourt College Publ, USA
46. Kim CS, Oh SM (2000) Importance of donor number in determining solvating ability of polymers and transport properties in gel-type polymer electrolytes. Electrochim Acta 45:2101–2109
47. Yang G, Hou W, Sun Z, Yan Q (2005) A novel inorganic–organic polymer electrolyte with a high conductivity: insertion of poly (ethylene) oxide into LiV_3O_8 in one step. J Mater Chem 15:1369–1374
48. Zhou W, Ma L, Lu K (2007) Facile Synthesis of polyaniline nanofibers in the presence of polyethylene glycol. J Polym Res 14:1–4
49. Kim D-W, Park J-K, Bae J-S, Pyun S-I (1996) Electrochemical characteristics of blended polymer electrolytes containing lithium salts. J Polym Sci B Polym Phys 34:2127–2137
50. Li Q, Sun HY, Takeda Y, Imanishi N, Yang J, Yamamoto O (2001) Interface properties between a lithium metal electrode and a poly (ethylene oxide) based composite polymer electrolyte. J Power Sources 94:201–205